Title
The Dynamics of Myxobacteria Life Cycle

Authors
Hendrata, Melisa
Birnir, Bjorn

Publication Date
2008-06-16

THE DYNAMICS OF MYXOBACTERIA LIFE CYCLE

Melisa Hendrata and Björn Birnir
Department of Mathematics
University of California, Santa Barbara

May 25, 2008

Abstract

We develop the off-lattice model to simulate the life cycle of *Myxococcus xanthus*. When the food is abundant, they grow as swarms that spread away from the colony. In this stage, their movement and coordination are determined by their A-motility and S-motility engines. However, when they are in starvation, C-signaling between cells takes place and changes their cell-cell coordination. This allows them to form an aggregate which eventually develops into a fruiting body. Cells inside the fruiting body differentiate into round nonmotile spores which are resistant to adverse condition. In this paper, the Dynamic Energy Budget model is used as a trigger mechanism for cell growth and cell division, and then for switching from the swarming stage to the stage of fruiting body formation. Moreover, the logistic equation is implemented to count the number of C-signal molecules on each cell surface, which is then used as a switch for transitions between the stages of fruiting body formation.

1 Introduction

Myxobacteria (*Myxococcus xanthus*) are flexible rod-shaped bacteria that are found mainly in the soil. The width:length ratio is approximately 1:10. The dimension of an average cell is 0.5-1.2μm by 2-12μm [10] [15]. Their social behavior exhibits complex multicellular interaction and organization which provides a prime model for studying the dynamics of cellular morphogenesis. In an ideal condition with sufficient amount of nutrient, myxobacteria grow as swarms that spread away from the center of a colony. However, when the nutrients are depleted, myxobacteria align and stream to form aggregates which later develop into round, nonmotile fruiting bodies within which the cells sporulate.

Myxobacteria have no flagella and thus are unable to swim. They move by gliding on solid surfaces [2]. There are two motility engines in a myxobacteria cell, namely the S(social)-motility and the A(adventurous)-motility. S-motility is driven by type IV pili that extend from the cell poles [19]. Studies found that the length of pili can reach up to one cell length [9]. Thus, when a cell is less than a pilus length apart from other cells, the pili can

reach out, retract, and pull the cell forward towards the group. A-motility is driven by the secretion of polysaccharide slime from nozzle-like organelles. These organelles are found at both poles and they secrete slime from one pole at a time. This propulsive force is due to the hydration-driven swelling of the polyelectrolyte slime in the nozzle [21]. Experiments also show that cells turn at acute angle and follow slime trails secreted by other cells [2]. Wild type (A+S+) myxobacteria cell possesses both A and S motility. The A+S- myxobacteria mutant possesses only the A-motility, while the A-S+ mutant possesses only the S-motility. A cell is motile if it possesses at least one of these types of motility. An isolated A-S+ cell is nonmotile, while an isolated A+S- cell is motile [6] [7]. A nonmotile cell that possesses neither A nor S-motility is denoted by A-S-. In addition to these motility engines, it was also found that myxobacteria reverse its polarity approximately every 10 minutes. During the polarity reversal, the motility engines are switched from pole to pole, which means that pili pulling and slime pushing on their current pole are switched off and become active on the opposite pole. [8].

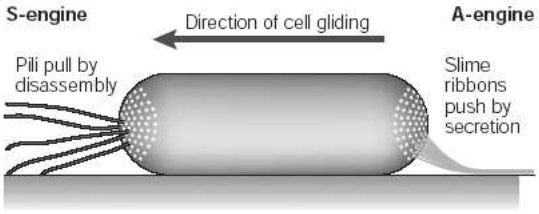

Figure 1: Motility engines in a myxobacteria cell. The S-engine is associated by pili on the head pole and the A-engine is associated by slime secretion on the posterior pole. Picture was taken from Kaiser (2003).

During starvation, life cycle of myxobacteria changes from the swarming stage to the stage of fruiting body formation. During this stage, the cells stop growing as individuals and the movement behavior of the cells changes. Fruiting body is initiated by starvation and built by cell movements and interactions. At least one motility engine is needed in fruiting body formation because A-S- mutants are unable to develop fruiting bodies [10]. The stages of fruiting body formation that are observed in the experiments consist of the formation of initial aggregates also known as traffic jams, streams, formation of hemispherical three-dimensional mounds, formation of toroidal mounds and sporulation within the fruiting body. This process is critical for the cells' survival during adverse condition.

Initially, cell aggregation was thought to be based on chemotaxis, a phenomenon in which cells' movements are directed by certain chemicals in their environment. Cells follow the maximal chemical gradient and tend to move towards the nearest and largest aggregates [20]. However, studies have found that in myxobacteria, cell aggregation and fruiting body formation are controlled by C-signal morphogen and is a result of direct cell-cell local inter-

actions [10]. The C-signal is a 17-kDa cell-surface protein that is transmitted by end-to-end contact between two cells [12]. Once C-signal molecule is inserted onto the cell surface, the proteins of the act operon increase the expression of the csgA gene. This in return increases the number of C-signal molecules that are exported to the cell surface of the signaling cells. Different levels of C-signal trigger different stages of the fruiting body formation [12]. In particular, when C-signal molecules have reached a certain threshold, the cell reduces the frequency of its polarity reversal and there is no polarity reversal in cells that are inside the aggregates [16]. When a pole of a cell hits another cell's pole, the two cells signal each other and increase their C-signal molecules on their cell surface. Furthermore, cells tend to move towards the direction in which the C-signal level is the highest.

There are two types of mathematical models that can be applied to biological problems, namely the continuous models and the discrete models. Two continuous models developed by Gallegos et al. were successful in analyzing the spreading rates of myxobacteria swarms on both short and long time scales [4]. One discrete model that has been highly developed is the Lattice Gas Cellular Automaton (LGCA) model. LGCA model discretizes space, time, and state, and represent a cell as a point in finite lattice along with local rules that determine cells' movements, interactions and transitions between states. Early lattice model succeeded in modeling the initial aggregation and stream formation [1] and a 3D stochastic LGCA model developed by Sozinova et al. was able to simulate the two stages of cell aggregation [17]. Later on, they developed a unified 3D model that successfully produced all stages of fruiting body formation [18]. In all of these simulations, it was shown that non-chemotactic cell-cell interactions are sufficient to produce the results [1] [17] [18].

In spite of the advancement in the development of LGCA model, the geometric constraint of the lattice has made this model artificial and inaccurate for quantitative analysis. In their paper, Wu et al. used a modified LGCA model to quantitatively describe the relationship between expansion rates and the initial density of the colony, and found that the overall expansion rate is much lower than the experimental result. To overcome this, the off-lattice model was then developed [22]. The off-lattice model is an improvement of LGCA model for which the cells are now free to bend and move in space.

In this paper, we present an off-lattice model that is a modification of the off-lattice model initially developed by Wu et al. Our model successfully produces the life cycle of myxobacteria based on non-chemotactic cell-cell interactions and its transition from the swarming stage to the stage of fruiting body formation. There are two components in our off-lattice model that play important role as the triggers in this transition. The first one is the Dynamic Energy Budget (DEB) model. This DEB model controls cell growth and cell division, and the switching from the swarming stage to the stage of fruiting body formation. The other component is the logistic equation that is used to keep track of the C-signal molecules, which then control the switching between the stages of fruiting body formation.

Dynamic Energy Budget (DEB) theory was first introduced by Kooijman to study the way organisms acquire and utilize their energy for somatic maintenance, growth and reproduction [13]. DEB model uses ODEs to solve for the internal energy density and the size of each

individual cell in the colony at any given time [13] [14]. The internal energy density is used as a trigger for the transition between the states of the cell. When a cell has high enough internal energy, it may grow or reproduce through cell division as regulated by its internal biological clock. However, when the internal energy goes below a certain threshold, the cell is in starvation and it enters the stage of fruiting body formation. The internal energy continues to play its role to control the cell's ability to climb over an aggregate and form the fruiting body.

In Section 2, we describe our off-lattice model in detail together with the modeling of A and S-motility and the collision handling mechanism. Section 3 consists of the algorithm and its analysis on the scaling of the parameters. We present our simulation results of the swarming stage for each type of myxobacteria cells (A+S+, A+S- and A-S+ mutants) and compare it with the experimental results to justify our algorithm. Section 4 explains the implementation of DEB model and C-signaling, and show how they function as trigger mechanisms. The algorithm and simulation result for each individual stage of the fruiting body formation are also presented in this section.

2 Off-Lattice Model

In off-lattice model, a cell is represented by a string of N nodes, where N varies between four to seven. Figure 2 shows a cell with 7 nodes with the black dots indicate the two poles of the cell. Even though a myxobacteria cell does not have a physical head and tail, we refer to the leading pole as the *head* node and the end pole as the *tail* node.

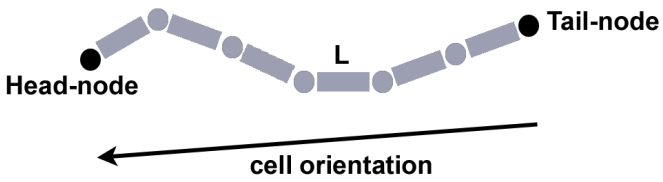

Figure 2: A cell with 7 nodes and the vector indicating its orientation.

There are (N-1) segments of equal length L, each of which connects two consecutive nodes. The vector pointing from the tail node to the head node determines the cell orientation along its long axis. Isolated A+S- or A+S+ cells moves along the direction of this orientation until they sense a slime trail or other cells nearby.

Biologically, during swarming stage the cells reverse their polarity roughly once in every 10 minutes [11]. To model this mechanism, we assign an internal clock for each cell which regulates its polarity reversal. During polarity reversal, the cell's tail-to-head orientation is reversed and we regard the head node as the tail node, and vice versa. This reversal process is independent of cell-cell interaction and collision. It is also known from experiments that a cell divides after 3 hours and it grows until it reaches its maximum length before it divides

[11]. Similar to polarity reversal, here we assign another internal clock for each cell that serves as a periodic timer for cell growth and cell division. If the cell has not reached its maximum length when this timer is on, the cell grows in length and the number of nodes of this cell is added by one. If the cell has reached its maximum when this timer is on, then the cell divides in the middle. The head and tail nodes of the original cell become the head nodes of the two new cells and the middle node of the original cell becomes the tail nodes of the new cells. The length of these new cells would be half of the length of the original cell. A schematic diagram in Figure 3 describes the cell division.

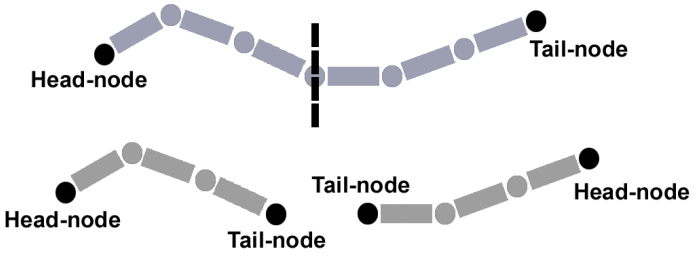

Figure 3: A cell with maximum length divides in the middle into two new cells with length half of the original length.

In this model we assume that cell movement is driven by the head node. This means that the head node determines where the cell will move to. The other nodes then get pulled forward following the head node. We also assume that a cell moves with a fixed step length which we take to be equal to one segment length L.

In absence of collision between cells, the direction to which a cell moves is determined by the A-motility direction, which consists of tail-to-head cell orientation and the direction due to slime trails, and the S-motility direction.

2.1 Modeling A-motility

The A-motility is driven by the secretion of slime from the nozzle-like organelles at the rear end. This slime secretion pushes the cell forward in the direction of the cell's tail-to-head orientation, which is given by the unit vector

$$\mathbf{C}_k = \frac{\mathbf{n}_{k1} - \mathbf{n}_{kN}}{\|\mathbf{n}_{k1} - \mathbf{n}_{kN}\|}, \tag{2.1}$$

where $\mathbf{n}_{k1}$ and $\mathbf{n}_{kN}$ are the vector position of the head and tail nodes of cell k, respectively.

As a cell moves forward, it leaves behind slime trails. In our simulation, we keep track of the cell position by keeping track of the position of each node. Likewise, we keep track of the slime trail by keeping track of the position of the slime points. In each iteration, the cell searches for slime points that is inside the searching circle. We define this searching circle to be the circular region around the head node with radius half of the cell length. This

searching circle determines how far a cell can sense the existence of slime trails deposited by other cells. Once a cell finds a slime point, we transform the coordinates of the slime point to determine the angle of the slime point relative to the cell's local coordinate system. A schematic illustration of coordinate transformation is shown in Figure 4.

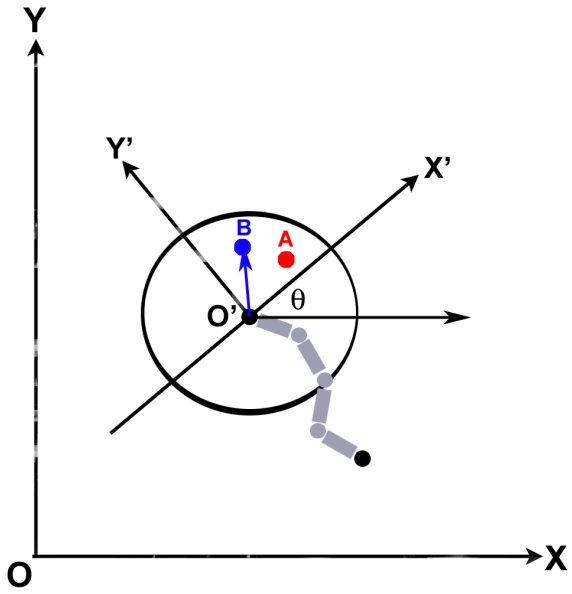

Figure 4: Coordinate transformation diagram. The cell's local coordinate is X'O'Y'. The circle around the head node indicates the searching circle.

The rotation matrix needed to transform the coordinates of the slime points is given by

$$\begin{bmatrix} \cos(-\theta) & -\sin(-\theta) \\ \sin(-\theta) & \cos(-\theta) \end{bmatrix}$$

where θ is the measure of how far the coordinate system XOY is rotated counterclockwise to get the cell's local coordinate system X'O'Y'.

If the slime point forms an acute angle with the positive X'-axis of the cell's local coordinate system, then the cell follows this slime point. Otherwise, it searches for another slime points inside the searching circle. If there are more than one slime points that satisfy this angle requirement, then the cell moves toward the slime point which was deposited the latest. This is based on the prediction that the newer slime trails have stronger effect than the older ones. In Figure 4, both slime points A and B form acute angles with positive X'-axis. If A is deposited at time t_A and B at time t_B, where $t_A < t_B$, then cell k moves towards the slime point B in the direction given by the unit vector

$$\mathbf{L}_k = \frac{\mathbf{s}_B - \mathbf{n}_{k1}}{\|\mathbf{s}_B - \mathbf{n}_{k1}\|}, \tag{2.2}$$

where $\mathbf{s}_B$ and $\mathbf{n}_{k1}$ are the vector positions of the slime point B and the head node of cell k, respectively.

Let α_k and β_k denote the weights of tail-to-head orientation and direction due to slime trail of cell k, respectively. Since the cell has the tendency to follow the slime trails, the algorithm first searches for the slime points nearby. If it finds at least one slime point within its searching circle that satisfies the angle requirement, then we set $\beta_k = 1$. Otherwise $\beta_k = 0$. The formula of the A-motility is given by

$$\mathbf{A}_k = \alpha_k \mathbf{C}_k + \beta_k \mathbf{L}_k, \tag{2.3}$$

where

$$\alpha_k = \begin{cases} 1 & \text{if } \beta_k = 0, \\ 0 & \text{if } \beta_k = 1. \end{cases} \tag{2.4}$$

2.2 Modeling S-motility

S-motility is the motility engine that is driven by type IV pili that extends from the cell's leading pole and whose length can reach up to one cell length. In modeling the S-motility, we define the vicinity of the pili to be the circular region centered at the head node with radius equal to the pili length. If there is a group of cell in this vicinity, then the pili can attach to the group and pull the cell towards it. Figure 5 shows a diagram of a cell with the circular vicinity of its pili.

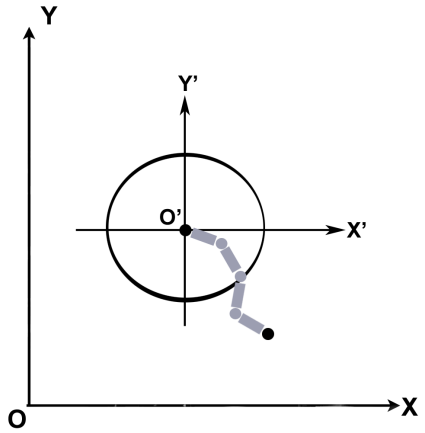

Figure 5: The S-motility diagram. The circular neighborhood around the head node indicates the vicinity of the pili.

We divide this pili vicinity of cell k into four quadrants. Each cell j that lies inside this circular region belongs to one of these quadrants. Cell k then counts how many distinct cells are in each quadrant. The quadrant that has the most number of distinct cells is chosen to be the region in which cell k will turn to. To determine cell k's direction for the next

iteration, we average the position angle of each cell j in this quadrant with respect to the head node of cell k. The S-motility direction of cell k is given by the formula

$$\mathbf{S}_k = \begin{bmatrix} \cos\alpha \\ \sin\alpha \end{bmatrix}, \quad \alpha = \frac{1}{N}\sum_{j=1}^{N} \phi_j, \tag{2.5}$$

where N is the number of distinct cells in the quadrant to which cell k is moving and ϕ_j is the position angle of cell j with respect to the head node of cell k, that is,

$$\begin{bmatrix} \cos\phi_j \\ \sin\phi_j \end{bmatrix} = \frac{\mathbf{r}_j - \mathbf{n}_{k1}}{\|\mathbf{r}_j - \mathbf{n}_{k1}\|}$$

with $\mathbf{r}_j$ and $\mathbf{n}_{k1}$ being the vector positions of cell j and head node of cell k, respectively.

As a consequence of this algorithm, the cell is likely to move in groups, in accordance with experiment.

2.3 Collision Handling Mechanism

In our simulation, we say the head node of cell k collides with a node of another cell j if the distance between them is less than a cell width. If collision happens, we use the following steps:

1. If the head node of cell k collides with a node of cell j other than the head node, then cell k randomly chooses to align its orientation with cell j's tail-to-head orientation or to stall until the next iteration.

2. If the head node of cell k collides with the head node of cell j, then the collision is resolved as follows:

   (a) Calculate the tail-to-head orientations for both cell k and j.

   (b) If the difference in angles between these orientations is close to 180 degrees (head-on collision), then cell k rotates its orientation 60 degrees away from the head node of cell j, and take this orientation as the new direction.

   (c) If not, then cell k randomly chooses to align its orientation with cell j or to stall until the next iteration.

3. If cell k hits the boundary of the domain, its tail-to-head orientation is reflected and this reflected orientation is taken as the new direction.

3 The Swarming Stage

3.1 Algorithm

In absence of collisions, the direction $\mathbf{V}_k$ in which cell k moves is determined by the A-motility and S-motility orientations described in the sections 2.1 and 2.2. We consider these

contributions as the weighted sum of the vectors $\mathbf{A}_k$ and $\mathbf{S}_k$ defined in (2.3) and (2.5). The general formula is given by

$$\mathbf{V}_k = \frac{\gamma_k \mathbf{A}_k + \delta_k \mathbf{S}_k}{\|\gamma_k \mathbf{A}_k + \delta_k \mathbf{S}_k\|}, \tag{3.1}$$

where γ_k and δ_k are the weights of A and S-motility term of cell k.

Wildtype A+S+ cells have both A and S-motility. Hence, in our simulation we take $\gamma_k = \delta_k = 1$. The A-S+ mutants only have the S-motility and we take $\gamma_k = 0$ and $\delta_k = 1$. On the other hand, the A+S- cells only have the A-motility and therefore we take $\gamma_k = 1$ and $\delta_k = 0$.

When there is a collision between cell k and its neighboring cells, then it moves according to the collision-handling mechanism as described in section 2.3, instead of its A and S-motility orientation $\mathbf{V}_k$.

3.2 Non-dimensionalization and Scaling

To analyze this off-lattice model, we need to consider the parameters that are involved in determining both A and S-motility directions. We can clearly see that the radius of the searching circle in A-motility and the length of the pili in S-motility algorithm are the two parameters to consider. We will discuss how these parameters scale as we scale the spatial and temporal resolutions in our simulation.

In off-lattice model we also assume that cell movement is driven by the head node. This means that the head node determines where the cell will move to. The other nodes then get pulled forward following the head node. In each iteration, cell k updates its position according to the discrete model

$$\mathbf{x}_k(t + \Delta t) = \mathbf{x}_k(t) + v\mathbf{V}_k(t)\Delta t + \vec{\epsilon}\, dB_t^k, \tag{3.2}$$

where Δt is the time step, $\mathbf{x}_k$ is the vector position of the head node of cell k, $\vec{\epsilon} dB_t^k$ is the white noise, v is the constant head velocity and $\mathbf{V}_k(t)$ is the weighted unit direction due to A and S-motility as defined in (3.1).

We nondimensionalize (3.2) by first noticing that $\mathbf{x}$, v and t are quantities with units. Let $[\mathbf{x}]$, $[v]$ and $[t]$ be the unit of measurement of $\mathbf{x}$, v and t, respectively. Then we have the relationships

$$\mathbf{x} = [\mathbf{x}]\mathbf{x}^*, v = [v]v^*, t = [t]t^*,$$

where $\mathbf{x}^*$, v^* and t^* are the dimensionless counterpart of $\mathbf{x}$, v and t, respectively. Ignoring the subscript k, the equation (3.2) now can be rewritten as

$$[\mathbf{x}]\mathbf{x}^*(t + \Delta t) = [\mathbf{x}]\mathbf{x}^*(t) + [v]v^*\mathbf{V}(t)[t]\Delta t^* + \vec{\epsilon}\, dB_t,$$

Dividing both sides of the equation by $[\mathbf{x}]$, we have

$$\mathbf{x}^*(t + \Delta t) = \mathbf{x}^*(t) + \frac{[v][t]}{[\mathbf{x}]}\mathbf{V}(t)v^*\Delta t^* + \frac{\vec{\epsilon}}{[\mathbf{x}]}\, dB_t, \tag{3.3}$$

For simplicity of notation, we drop the superscript * and keep in mind that the variables $\mathbf{x}$, v and t are now unitless. By setting

$$a = \frac{[v][t]}{[\mathbf{x}]}, \quad b = \frac{1}{[\mathbf{x}]},$$

we obtain the dimensionless equation

$$\mathbf{x}(t + \Delta t) = \mathbf{x}(t) + a\mathbf{V}(t)v\Delta t + b\vec{\epsilon}\, dB_t. \tag{3.4}$$

We now see how the parameters scale in relation to one another. From equation (3.4), one can deduce the simple relationship

$$\Delta x = v\Delta t + \epsilon^* dB_t, \tag{3.5}$$

where Δt is the time step, Δx is the distance a cell travels in one time step, ϵ^* is the noise magnitude and v is the head velocity of a cell, which is kept constant in our simulation. In our simulation Δt and Δx are the temporal and spatial resolutions, respectively. Note that if we scale Δx by a factor α, then we also need to scale Δt and ϵ^* by the same factor as well, that is,

$$(\alpha\Delta x) = v(\alpha\Delta t) + (\alpha\epsilon^*)dB_t,$$

which means Δx, Δt and ϵ^* scale linearly

$$\Delta t \sim \Delta x \sim \epsilon^*. \tag{3.6}$$

Now let r_s denote the radius of the searching circle in the A-motility algorithm and r_p the length of pili in the S-motility algorithm described in section 2.1 and 2.2, respectively. These parameters then also scale linearly with the spatial resolution Δx:

$$\Delta x \sim r_s \sim r_p. \tag{3.7}$$

The next question is how to find the scaling factor α for a particular simulation given a reference simulation with certain parameter values. We start by considering a domain of area A, which we divide into small squares, each of which has side equals to Δx. Let N be the number of cells in an actual laboratory experiment. As this quantity is very big, we regard each cell in the simulation as a *superindividual*. Each superindividual cell represents a certain number of cells in the actual experiment. Let n be the number of superindividual cells in a square. Then the density of this square is given by

$$\rho = \frac{n}{\Delta x^2}.$$

Assuming the density is uniform throughout the entire domain and the number of superindividuals in a square is fixed, then the total number of superindividuals in our simulation is

$$n_T = \frac{nA}{\Delta x^2}$$

and the number of cells each superindividual represents is given by

$$\beta = \frac{N}{n_T} = \frac{N\Delta x^2}{nA}. \tag{3.8}$$

Ideally, to capture the cell's individual behavior and its interaction with other cells, one would like to have $\beta = 1$. In other words, an individual cell in the simulation represents one cell instead of a group of cells in the actual experiment. Hence, it is desirable to keep β as small as possible and consider how β scales in relation to Δx. From (3.8), we obtain the relationship

$$n = \frac{N\Delta x^2}{\beta A}. \tag{3.9}$$

We would like to keep n constant regardless of the spatial resolution. Here, N and A are also fixed. Let Δx_0 and β_0 denote the spatial resolution and the number of cells represented by a superindividual in a reference simulation, respectively. Since n is constant, the equation (3.9) gives us the relationship

$$\frac{N\Delta x^2}{\beta A} = \frac{N\Delta x_0^2}{\beta_0 A},$$

which implies

$$\Delta x = \sqrt{\frac{\beta}{\beta_0}}\Delta x_0.$$

Thus, we set the scaling factor

$$\alpha = \sqrt{\frac{\beta}{\beta_0}}. \tag{3.10}$$

3.3 Simulation Results

To test our algorithm and see the impact of the A-motility, S-motility, or combination of both on the global behavior of myxobacteria during swarming stage, we simulate each A+S+, A-S+, and A+S- colony separately. For each of these types, we randomly distribute 300 cells in a circular colony. In these simulations we also include polarity reversal, cell growth and division. We observe and compare our simulations result to those obtained from experiments.

Figure 6 shows the swarming pattern of A+S+ myxobacteria colony. The cells move outwards away from the colony. They do not grow uniformly in all radial directions, but instead they form peninsulas. Some groups of cells separate themselves from the colony edge and form rafts of cells. We can also find single cells that travel away from the colony. Usually both single cells and rafts of cells eventually merge with the peninsulas.

Figure 7 shows the swarming pattern of A-S+ myxobacteria colony. The peninsulas of A-S+ cells are similar to those of A+S+ cells. However, since an individual A-S+ cell can only move when it is close enough to another cells, the cells in the colony tend to move in groups. Hence, the peninsulas of A-S+ cells are shorter, thicker and shaped like arrowheads.

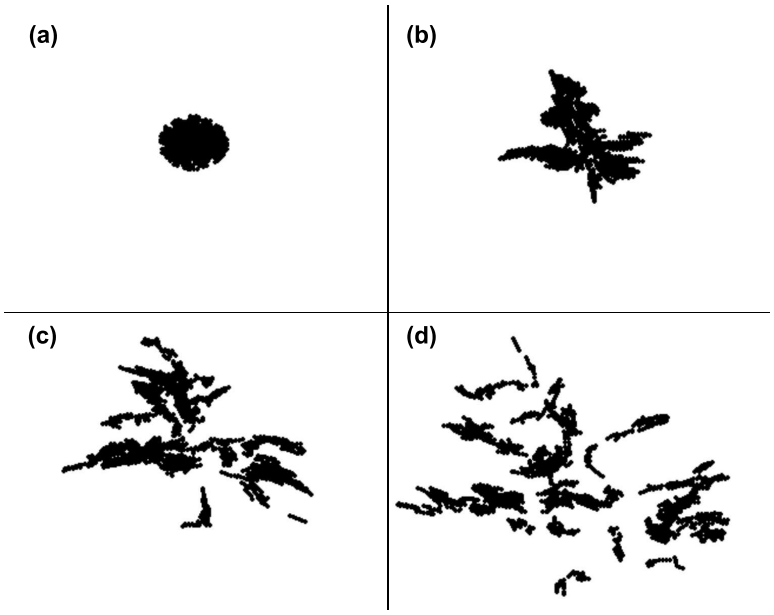

Figure 6: (a) Initial colony consisting of 300 A+S+ cells. (b) After 30 iterations, cells start to move outwards away from the center of the colony. (c) After 60 iterations, cells move in groups, forming peninsulas and rafts of cells. (d) After 100 iterations, swarms of A+S+ cells exhibit complex patterns.

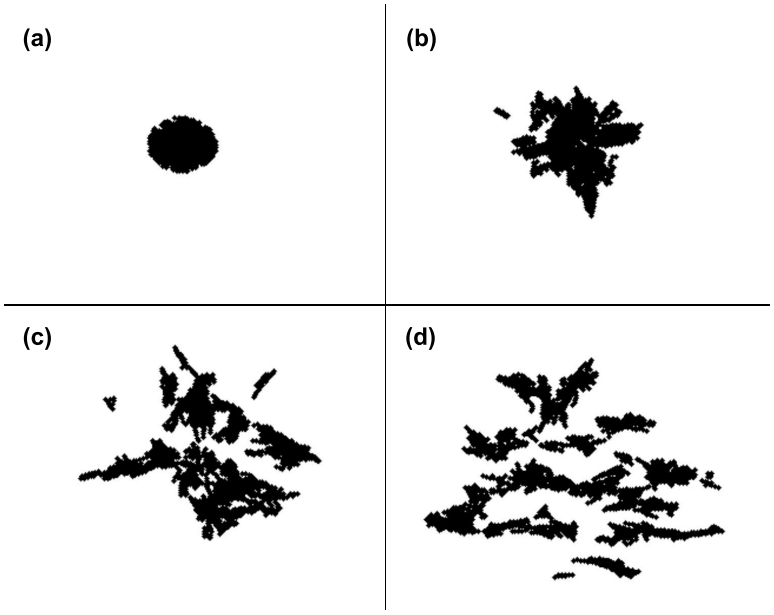

Figure 7: (a) Initial colony consisting of 300 A-S+ cells. (b) After 30 iterations, cells start to move outwards in groups, away from the center of the colony. (c) After 60 iterations, some thicker and shorter peninsulas start to form. (d) After 100 iterations, we have a swarm of A-S+ cells in the form of arrowhead-shaped peninsulas.

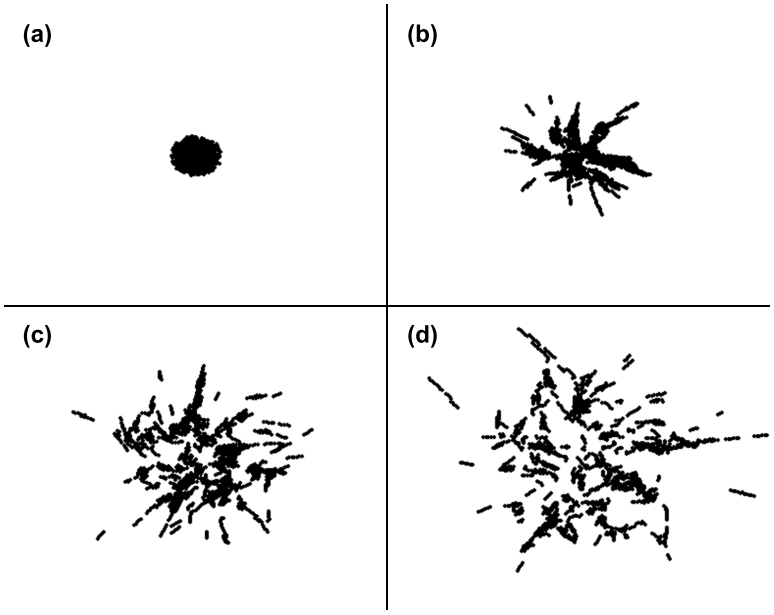

Figure 8: (a) Initial colony consisting of 300 A+S- cells. (b) After 30 iterations, cells move outwards in radial direction, forming thin and long peninsulas. (c) After 60 iterations, peninsulas grow bigger as some smaller peninsulas and rafts of cells have merged. (d) After 100 iterations, we have a swarm of A+S- cells consisting of peninsulas, rafts of cells, and single cells that travel away from the center of the colony.

These arrowhead-shaped groups tend to move away from each other. A group may split into several groups and we can see the number of groups increases in time.

Figure 8 shows the swarming pattern of A+S- myxobacteria colony. Similar to A+S+ mutants, the A+S- cells grow outwards in the form of peninsulas. However, the peninsulas of A+S- mutants are relatively narrower than those of A+S+ and A-S+ mutants. Some single cells or group of cells may travel away from the colony, but some may eventually rejoin the peninsulas.

We compare our simulation results with those obtained from the experiments in Figure 9. The top row of Figure 9 shows the experimental results of A+S+, A+S- and A-S+ mutants swarming patterns, while the bottom row shows the simulation results at the 100th iteration. We can see that our simulations agree with experimental observations and this agreement justifies our algorithms for the swarming stage.

4 The Fruiting Body Formation

Myxobacteria changes its life cycle from the swarming stage to the stage of fruiting body formation according to food availability in its environment. When the food supply is abundant, the food uptake is optimal and the cells' internal energy increases. When this internal energy reaches the maximum, the cells grow to its maximum length and reproduce through

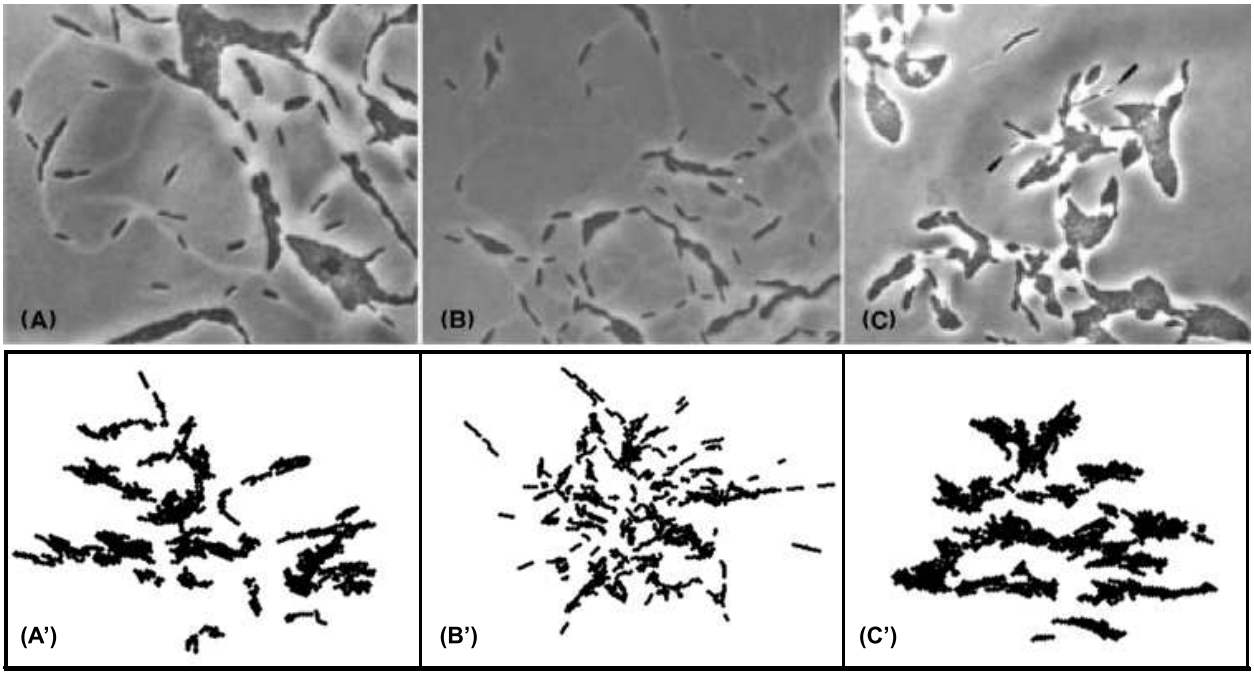

Figure 9: The top and bottom rows show laboratory observations and simulation results, respectively, of the (A,A') A+S+ strain, (B,B') A+S- strain, (C,C') A-S+ strain. Pictures were taken from Wolgemuth (2002).

cell division. Lack of nutrient causes their internal energy to decrease and eventually this prohibits their ability to grow and reproduce. We describe this relationship by utilizing the Dynamic Energy Budget (DEB) model, which will be discussed in detail in section 4.1.

During the fruiting body formation, the cells not only stop growing due to the decrease in their internal energy, but they also change their movement and coordination. The changes are due to the C-signaling between cells that occur when two cells are in end-to-end contact. During the stages of fruiting body formation, the cells tend to move towards the direction that would increase the likelihood of C-signaling event. With each C-signaling event, the number of C-signal molecules on the cell surface increases. Different levels of C-signal molecules trigger different stages of fruiting body formation. In section 4.2 we discuss about the logistic equation that can be used to model this C-signaling and how it triggers the changes in the stages of fruiting body formation.

4.1 Dynamic Energy Budget (DEB) Model

Dynamic Energy Budget (DEB) uses ODEs to describe the rates at which cells acquire and utilize energy for somatic maintenance, growth and cell division. These rates depend on the length of the cell and the food density. Hence, once incorporated, this DEB model can be used as trigger mechanism from the stage where the food is plenty to the starvation stage, namely the transition from the swarming stage to the stage of fruiting body formation. We

use the following DEB model taken from Nisbet et al. [14]:

$$\frac{dL}{dt} = \frac{\dot{\nu}}{3}\frac{(E/E_m) - (L/L_m)}{g + (E/E_m)} \tag{4.1}$$

$$\frac{dE}{dt} = \frac{A_m}{L}\Big(f - \frac{E}{E_m}\Big) \tag{4.2}$$

where the primary parameters are

$$\begin{aligned}
E &= \text{internal energy density} \\
L &= \text{cell length} \\
X &= \text{food density} \\
\kappa &= \text{fraction of utilized energy spent on maintenance and growth} \\
K &= \text{saturation coefficient} \\
G &= \text{energy costs for a unit increase in size} \\
E_m &= \text{maximum storage energy} \\
L_m &= \text{maximum cell length} \\
A_m &= \text{maximum assimilation rate}
\end{aligned}$$

and the compound parameters are defined as follows

$$\begin{aligned}
f &= \frac{X}{K + X} \\
\dot{\nu} &= \text{energy conductance: } \frac{A_m}{E_m} \\
g &= \text{investment ratio: } \frac{G}{\kappa E_m}
\end{aligned} \tag{4.3}$$

We non-dimensionalize the above system of ODEs by introducing new variables

$$L^* = L/L_m, \quad E^* = E/E_m. \tag{4.4}$$

Then $L = L^* L_m$ and $E = E^* E_m$, and it follows that

$$\frac{dL}{dt} = \frac{dL^* L_m}{dt}, \quad \frac{dE}{dt} = \frac{dE^* E_m}{dt}. \tag{4.5}$$

By (4.1), (4.2), (4.4) and (4.5), we now have

$$\begin{aligned}
\frac{dL^*}{dt} &= \frac{1}{L_m}\frac{dL}{dt} = \frac{\dot{\nu}}{3L_m}\Big(\frac{E^* - L^*}{g + E^*}\Big) \\
\frac{dE^*}{dt} &= \frac{1}{E_m}\frac{dE}{dt} = \frac{A_m}{E_m L}(f - E^*)
\end{aligned}$$

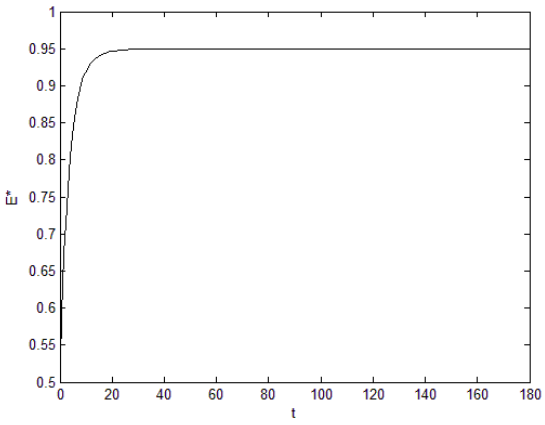

Figure 10: Graph of E^* vs. t

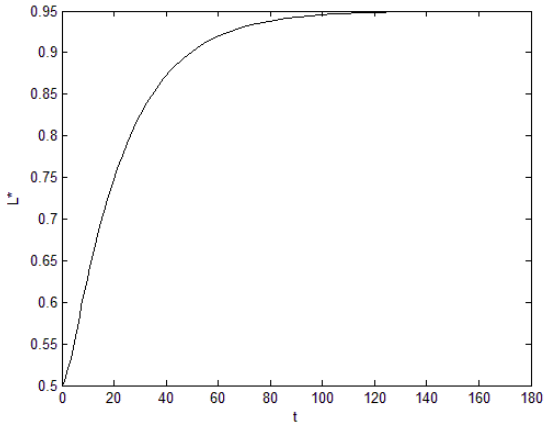

Figure 11: Graph of L^* vs. t

By (4.3) and (4.4), the non-dimensional DEB model now becomes

$$\frac{dL^*}{dt} = \frac{\dot{\nu}}{3L_m}\Big(\frac{E^* - L^*}{g + E^*}\Big) \tag{4.6}$$

$$\frac{dE^*}{dt} = \frac{\dot{\nu}}{L^* L_m}(f - E^*) \tag{4.7}$$

From the graphs of E^* and L^* versus t, we see that the values E^* and L^* approach a limiting value that is equal to f. We first choose a value for f and by using some experimental data on cell division, we estimate $\dot{\nu}$ from (4.7) and then g from (4.6).

Assuming the food is sufficient, a cell divides after it reaches the maximum length and roughly once in every three hours, which we take to be equal to 180 time steps in our simulation. We also assume that the cell's internal energy has to be close to the maximum in order to divide. Hence, we choose f to be a fraction close to 1. Here we take $f = 0.95$. From the graph E^* versus t, we estimate the value for $\dot{\nu}$ such that E^* reaches 0.95 for t close to 180. Having estimated $\dot{\nu}$, we use the graph of L^* versus t to estimate g such that L^* approaches 0.95 as t approaches 180. The graphs of E^* and L^* versus t are shown in Figure 10 and 11. Here we found the following estimates

$$g \approx 0.1, \quad \dot{\nu} \approx 0.15$$

which we will use in our simulation.

We note that f is an increasing function of X. Hence, the decrease of X leads to the decrease of f and eventually the decrease of E^*. We set the minimum internal energy for the cell motility to be 0.001. For each cell displacement, we numerically solve (4.6) and (4.7) for E^* and L^* by using the 4th-order Runge-Kutta method [3]:

$$
\begin{aligned}
k_1 &= h\mathbf{f}(t_i, \mathbf{y}_i) \\
k_2 &= h\mathbf{f}\Big(t_i + \frac{h}{2}, \mathbf{y}_i + \frac{k_1}{2}\Big) \\
k_3 &= h\mathbf{f}\Big(t_i + \frac{h}{2}, \mathbf{y}_i + \frac{k_2}{2}\Big) \\
k_4 &= h\mathbf{f}(t_{i+1}, \mathbf{y}_i + k_3) \\
\mathbf{y}_{i+1} &= \mathbf{y}_i + \frac{1}{6}(k_1 + 2k_2 + 2k_3 + k_4),
\end{aligned}
$$

where $\mathbf{f}$ is the right hand side of (4.6) and (4.7) and $\mathbf{y}_0 = (L^*(0), E^*(0))$ is the initial condition. Note that dL^*/dt cannot be negative as the physical length of a cell cannot decrease. Thus, (4.6) gives us the restriction $E^* \geq L^*$. When this is not the case, we take f to be the right hand side of (4.7) and keep L^* constant. Cell growth and cell division cost more energy than cell motility, and thus we reduce E^* by some preset amounts when they happen.

4.2 C-Signaling

During the fruiting body formation, the cells change their movement behavior and cell-cell interaction and coordination. The changes is due to the C-signaling between cells that occur when two cells are in end-to-end contact. With each C-signaling event, the number of C-signal molecules on the cell surface increases and the rate at which it is increasing is given by the logistic equation

$$
\frac{dN}{dt} = \frac{cN(N_{\max} - N)}{N_{\max}}, \tag{4.8}
$$

where N is the current number of C-signal molecules on the cell surface, $N_{\max}$ is the maximum number of C-signal molecules at the time of sporulation and c is the logistic constant.

It is known that there is on average a few C-signal molecules per cell and this number increases up to several hundred molecules when the cell starts to sporulate [5]. In our simulation we set a random integer between 10 to 20 for the initial number of C-signal molecules that a cell has. Once a cell enters the stage of fruiting body formation, it checks whether its poles (head or tail nodes) hit another cell's pole. If it does, then we solve (4.8) numerically by using the 4th-order Runge-Kutta method [3] to compute the number of molecules after this signaling event. In a particular iteration, a cell can C-signal with at most two other cells–one at the head node and the other at the tail node.

During the development of the fruiting body, the cells tend to move in the direction that increases the likelihood of C-signaling event. Different levels of C-signal induce different stages of fruiting body formation [5] [12]. These stages are the formations of aggregate, three-dimensional hemispherical mound, toroidal mound and finally sporulation within the fruiting body. We set different thresholds of the total number of C-signal molecules in this

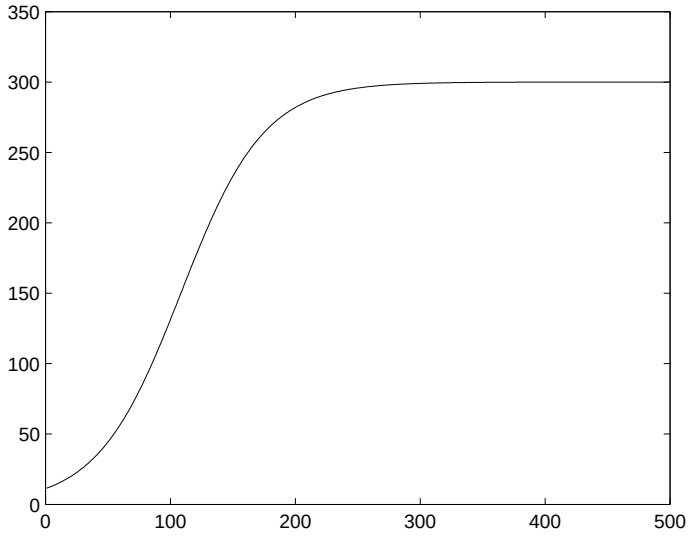

Figure 12: The logistic equation with $c = 0.03$ and $N_{\max} = 300$

population of cells for each of these stages. When this number passes a certain threshold, the cells change their movement accordingly. The cells within the fruiting body continue to C-signal until their individual C-signal level has reached the final threshold for its differentiation into spores.

4.3 Algorithm and Simulation Results

Our simulation starts from the swarming stage where the food is abundant and switches automatically to the fruiting body stage as the food is depleted. The stages of fruiting body formation consist of the aggregation, the formations of hemispherical mound, toroidal mound and the sporulation. The algorithm and simulation result for each substage are discussed and presented in this section.

4.3.1 Swarming Stage

We initially start with a circular colony consisting of 300 A+S+ myxobacteria cells, each of which has a random internal energy E^* between 0 and 1, length L^* between 0.5 and 1 and C-signal molecules between 10 to 20. We maintain the cell density such that the density of the domain is roughly the same for all time by adding a certain number of cells from the boundary. This is also necessary as enough number of cells must be present in order to complete a fruiting body.

To see how the DEB equations (4.6)-(4.7) function as a trigger mechanism from the swarming stage to the stage of fruiting body formation, we first set the food density $X = 20$ and the saturation coefficient $K = 0.25$. This gives $f = X/(X + K) \approx 0.98$ to start off. We

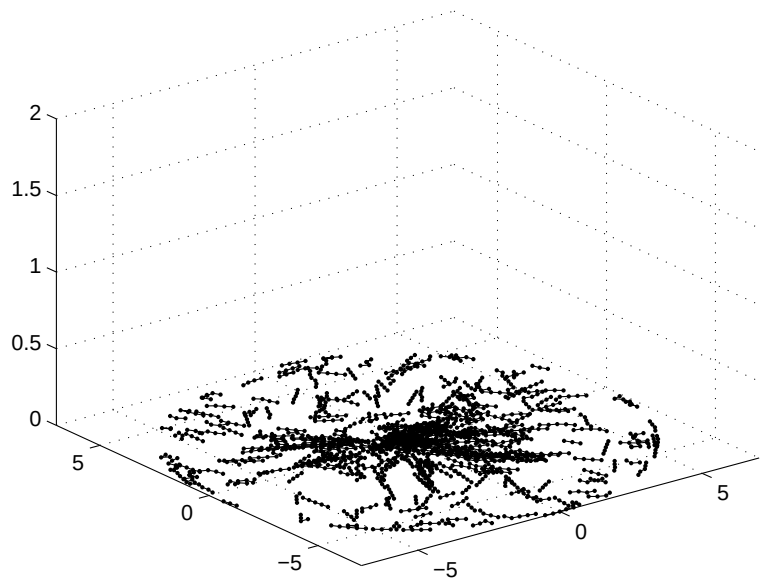

Figure 13: A colony of A+S+ cells are in the swarming stage during the first 35 iterations.

keep these values constant for the first few iterations so that the cells' internal energy E^* can increase and allows some of them to grow and divide. Most cells are in the swarming stage at this point and they move according to the algorithm described in section 3.1. Figure 13 shows the cells in this swarming stage move outward away from the colony in forms of peninsulas and rafts of cells.

4.3.2 Aggregation

After keeping X constant for a few iterations, we now decrease X by 5% in every time step. This would decrease f and cause E^* to start decreasing as well. If the internal energy E^* of a cell is above a certain threshold, then the cell is still in the swarming stage and it follows the algorithm in section 3.1. When E^* goes below a certain threshold, the cell is in starvation and it executes the first stage of fruiting body formation, which is the aggregation. At this stage, C-signal protein on the cell surface becomes active and cells tend to move towards the area with higher cell density to increase the likelihood of C-signaling. Once two cells C-signal each other, they tend to move together as a chain and this triggers the formation of streams entering the aggregate.

The effect of A-motility in this stage is much smaller than S-motility and C-signaling. Hence, our algorithm for this stage is very similar to the S-motility algorithm in section 2.2 with some modifications to accommodate the effects from A-motility and C-signaling. The algorithm considers both local and global cell interactions as follows

- *Local cell interaction:* Cell k aligns its orientation with orientations of other cells in its

pili vicinity area. The pili vicinity area is the circular region around the head node as shown in Figure 5. If $\mathbf{C}_k$ and $\mathbf{C}_j$ defined in (2.1) are tail-to-head orientations of cell k and j, respectively, then the new direction for cell k according to local interaction rule is given by

$$\mathbf{S}_k = \frac{1}{N} \sum_{j=1}^{N} \frac{\widehat{\mathbf{C}}_j}{\|\widehat{\mathbf{C}}_j\|}, \tag{4.9}$$

where N is the number of cells within the pili vicinity area of cell k and $\widehat{\mathbf{C}}_j$ is the vector following the rule:

- If $\mathbf{C}_k \cdot \mathbf{C}_j < 0$, then $\widehat{\mathbf{C}}_j = -\mathbf{C}_j$
- If $\mathbf{C}_k \cdot \mathbf{C}_j \geq 0$, then $\widehat{\mathbf{C}}_j = \mathbf{C}_j$

- *Global cell interaction:* Cell k moves towards the most crowded region to increase the likelihood of C-signaling. This global interaction is very similar to the S-motility. The only difference is that the vicinity of cell k now covers the entire domain. Cell k divides its global vicinity centered at its head node into four quadrants as shown in Figure 5. Then it counts how many cells are in each quadrant. Cell k then picks a random direction in the most crowded quadrant.

Having two new directions due to local and global interactions, cell k then randomly chooses one of these two directions to be its next direction. Figure 14 shows the result of this algorithm. Cells form an aggregate that quickly absorb nearby cells that are already in the starvation stage. Due to C-signaling, the cells tend to move together as a chain and this results in the formation of streams that enter the aggregate.

As the aggregate grows larger and denser, the cells in the center are unable to move. They form a traffic jam and become the nucleus of the aggregate. As the incoming cells are unable to penetrate this traffic jam, they move around along its boundary. To make our algorithm more efficient for this particular stage, we compute the cell density for each cell. Cell density of cell k is the number of other cells whose distance is less than half of a segment length from the head or tail node of cell k. If the cell density is higher than a certain number, then cell k "freezes". These frozen cells form the traffic jam in the center of the aggregate. Other incoming motile cells also check the cell density to determine how they approach this aggregate. If the cell density is below a certain threshold, it then enters the aggregate. On the other hand, if it is above the threshold, it then moves around along the boundary of the aggregate. As a result, this aggregate starts to round up as seen in Figure 15.

4.3.3 Hemispherical Mound

As the cells circulate around the aggregate, they continue to C-signal. When the level of C-signal molecules of the population passes a certain threshold, the formation of three-

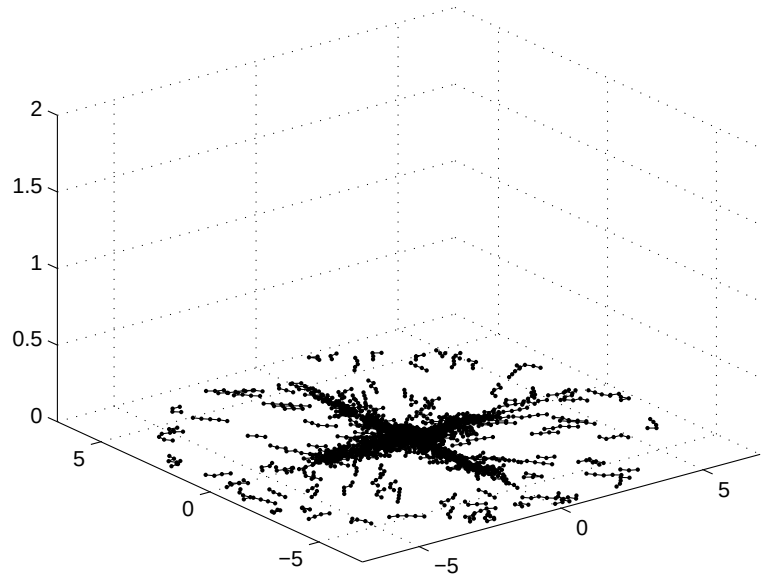

Figure 14: Cells begin to starve and enter the first stage of fruiting body formation as the food density is decreased. An aggregate and streams entering the aggregate is shown after 125 iterations.

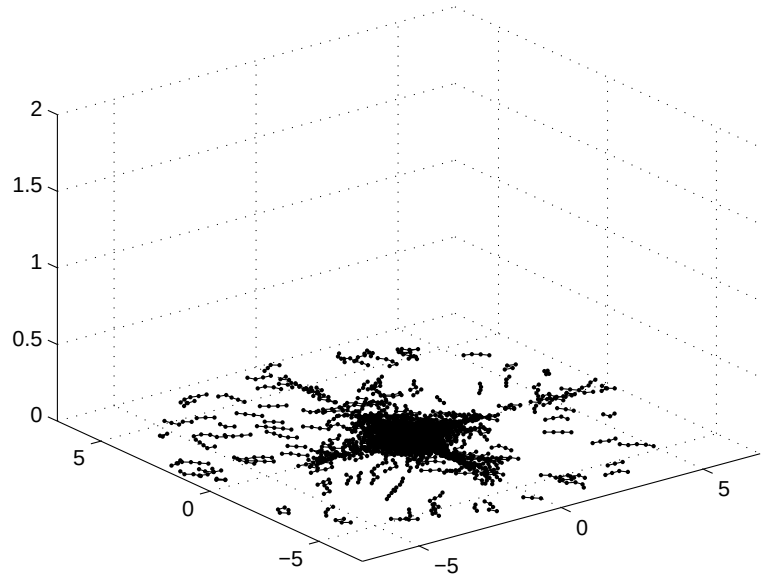

Figure 15: Incoming cells that are unable to penetrate the traffic jam move around along the boundary of the aggregate.

dimensional hemispherical mound begins. Some of the cells may climb over the aggregate and eventually cover up the traffic jam.

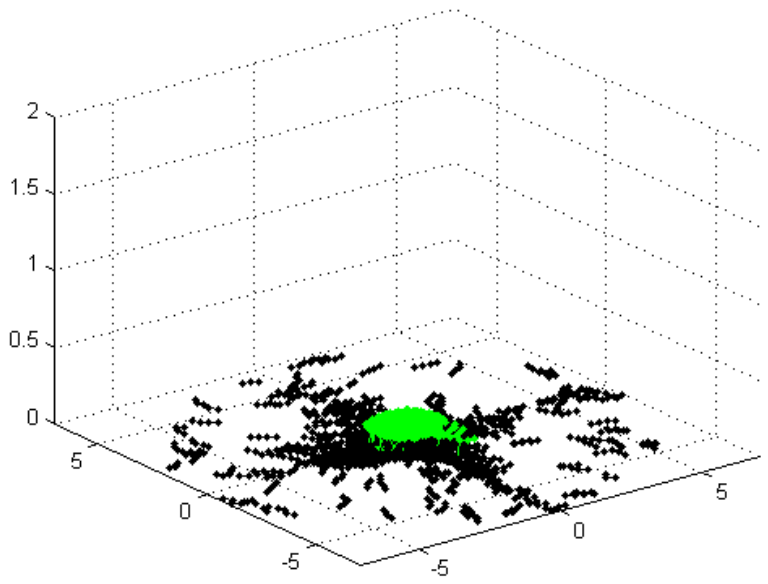

Figure 16: The early formation of three-dimensional hemispherical mound after 200 iterations. The green color indicates the cells are on the second layer of the mound.

At this stage, in addition to computing cell density, our algorithm also checks the internal energy E^*. If a cell hits the traffic jam and it has high enough cell density and internal energy, then it climbs over the traffic jam. Otherwise, it circulates around the boundary of the aggregate. In Figure 16, the cells colored in green are those that climbed up and are in the second layer of the mound, while the black ones are those that are still on the bottom layer. When a cell climbs up the aggregate, we also reduce its internal energy E^* by some constant. When $E^* < 0.001$, the cell stalls.

Similarly, once a cell is in an upper layer of the hemisphere, it again checks for the cell density in the same layer and its internal energy. This is needed to make sure the number of cells in this layer is less than the number of cells in the layer below it. If this particular layer is dense enough, then cells who have sufficient internal energy may climb up to the layer above it. In addition, the cells also continues to C-signal with other cells in the same layer. The aggregate stops growing once a hemispherical mound is formed as shown in Figure 17.

4.3.4 Toroidal Mound

The motile cells continue to circulate in both clockwise and counterclockwise direction around the aggregate. When the total number of C-signal molecules of the population reaches a certain threshold, the frozen cell on the bottom layer of the aggregate that is adjacent to

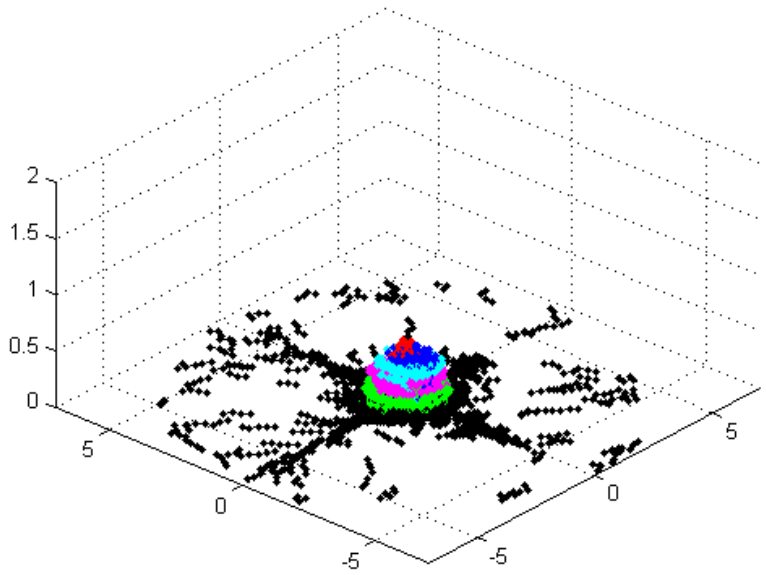

Figure 17: The hemispherical mound consisting of six layers (including the bottom layer). Different colors indicate different layers.

these motile cells aligns its orientation with the orientations of the motile cells and begins to move. This movement would unfreeze the other frozen cells adjacent to it. Eventually the traffic jam in the base layer of the mound is resolved. The cells move in circular orbit and due to some randomness in their direction, a hole in the middle of the base layer opens up.

The cells in the upper layers follow the movement of the cells on the layer below them. This causes a hole to open up in the upper layers as well. The hemispherical mound now becomes a fruiting body with hollow center. This hole becomes the site of spore accumulation in the next stage. In Figure 18, we can see the internal structure of this toroidal mound. The three-dimensional view is shown in Figure 19.

4.3.5 Sporulation

C-signaling continues while cells are moving in circular orbit within the annulus. The level of C-signal molecules on each cell surface increases until it reaches a final threshold of sporulation. During sporulation, the cell differentiates into spore by shortening and rounding up its rod-like cell body. Figure 20 shows a schematic diagram of spore differentiation mechanism in our simulation. The head node of a cell becomes the center node of the spore, while the other nodes of the cell becomes the boundary nodes of the round spore.

Myxospores are unable to move on their own. The ones on the bottom layer can only move passively by being pushed by other motile cells into the middle hole. This is implemented by checking whether there is a collision between a spore and a motile cell. If there is, then

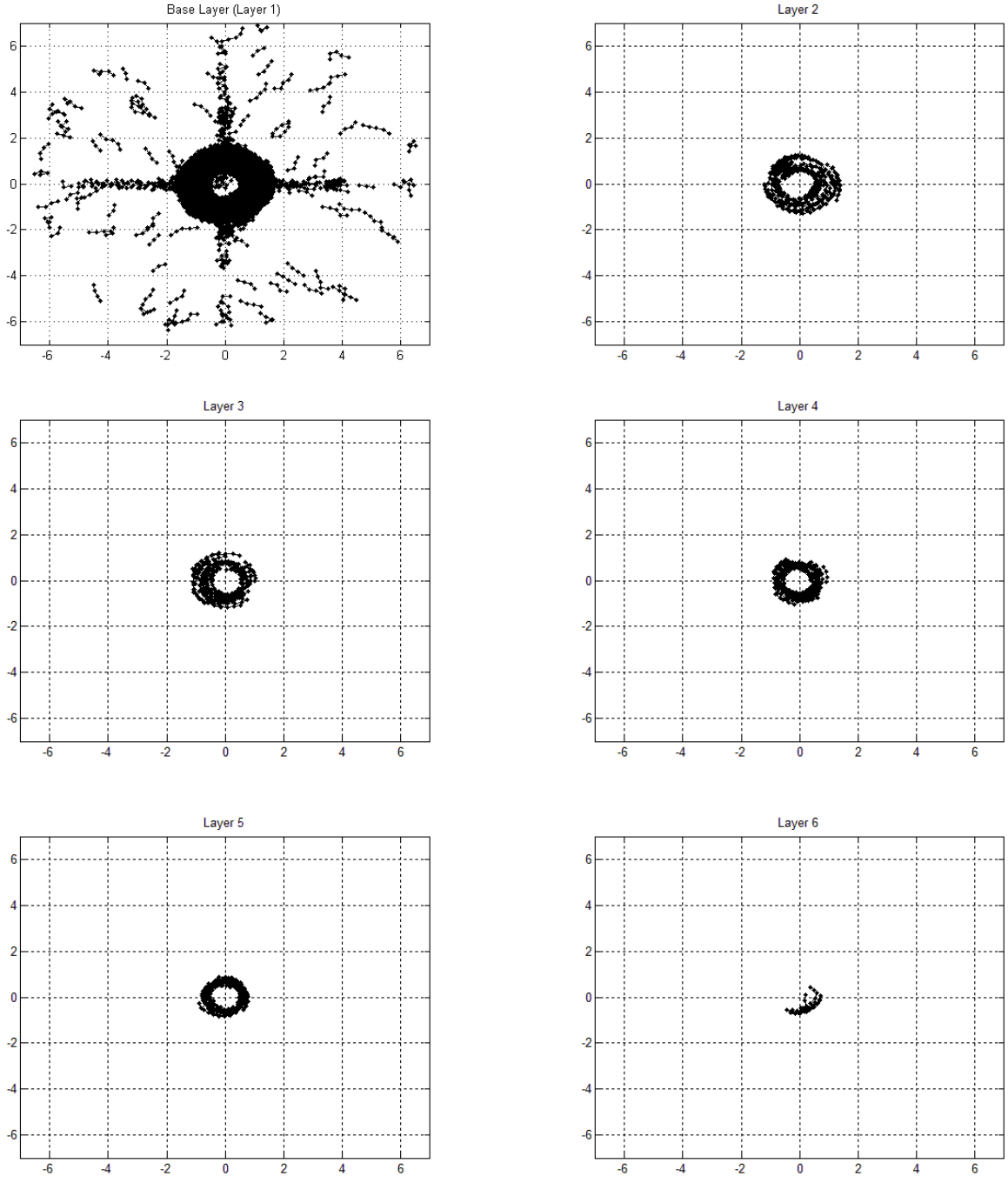

Figure 18: The internal structure of toroidal mound.

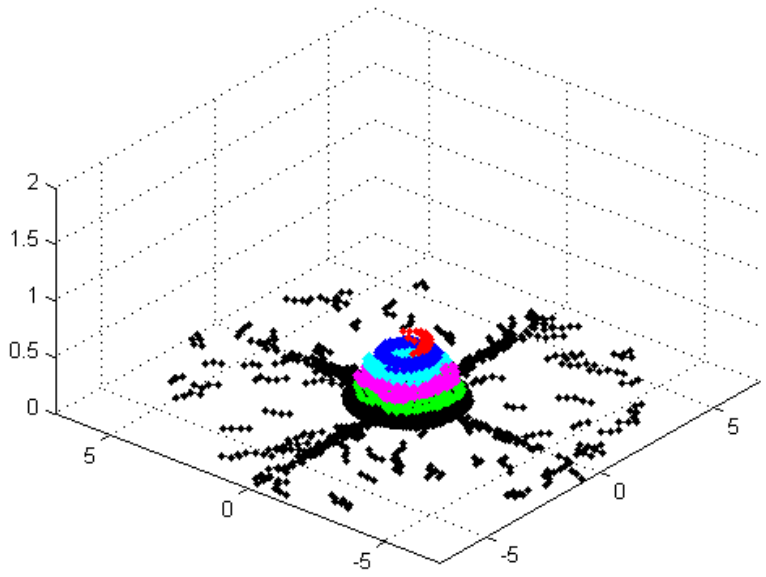

Figure 19: The toroidal mound is formed as the traffic jam in the bottom layer is resolved and the cells move in circular orbit.

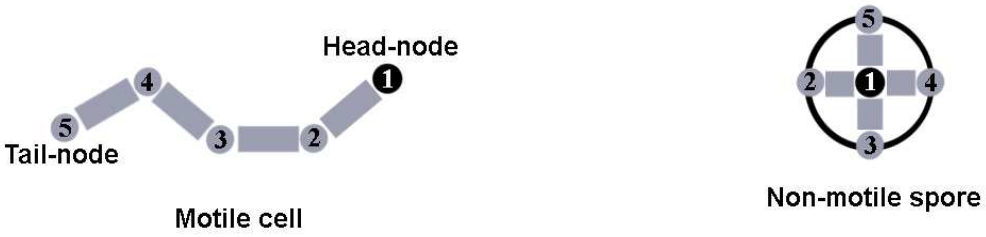

Figure 20: A rod-like cell differentiates into a round spore whose radius is half of a segment length. The head-node of the cell becomes the center node of the spore.

the spore is displaced as far as its diameter towards the middle hole. The motile cell keeps circulating on its orbit.

As more cells differentiate into spores and fill up the middle hole, some of these spores get pushed up and fill in the holes in the upper layers of the fruiting body. These transported spores eventually fill up the hollow center and are called the *inner spores*. The cells on the upper layer that differentiated into spores stay on the boundary and become the *outer spores*. Figure 21 shows the internal structure of a mature fruiting body. The spores colored in red are the outer spores, while the green ones are the inner spores. Figure 22 shows its three-dimensional view with the spores colored in red.

5 Conclusion

With the off-lattice model, we attempt to eliminate the geometric constraints of the LGCA model and produce results similar to those observed in laboratory experiments. The off-lattice model allows a cell to bend and occupy any space in the domain. We developed the A and S-motility algorithms for this model and we showed that it can simulate the swarming patterns of A+S+, A+S- and A-S+ myxobacteria cells. We analyze its discrete model to find the scaling between the spatial and temporal resolution in the simulation and also their relationship with other parameters in the model.

We developed the algorithm to produce all stages of the fruiting body formation starting from the initial aggregation up to the sporulation based on non-chemotactic cell-cell interactions. The Dynamic Energy Budget (DEB) model is incorporated in our off-lattice model to control cell growth and cell division during the swarming stage, and later to automatically do the transition to the stage of fruiting body formation when the cells undergo starvation. The logistic equation is also implemented to count the number of C-signal molecules of each cell surface. As the total number of C-signal molecules passes a certain threshold, the population switches from one stage to another stage of the fruiting body formation. During these stages, the number of C-signal molecules of each individual cell also increases and eventually reaches a final threshold for sporulation. The cell then differentiates into spore and a mature fruiting body consisting of motile round spores are formed.

References

[1] M. S. Alber, M. A. Kiskowski, Y. Jiang, *Two-stage aggregate formation via streams in myxobacteria*, *Physical Review Letters*, The American Physical Society, Volume 93, Number 6, August 2004.

[2] R. P. Burchard, *Trail following by gliding bacteria*, J. Bacteriology, 152, 495-501, 1982.

[3] R. L. Burden, J. D. Faires, *Numerical Analysis*, 7th ed., Brooks/Cole, 2001.

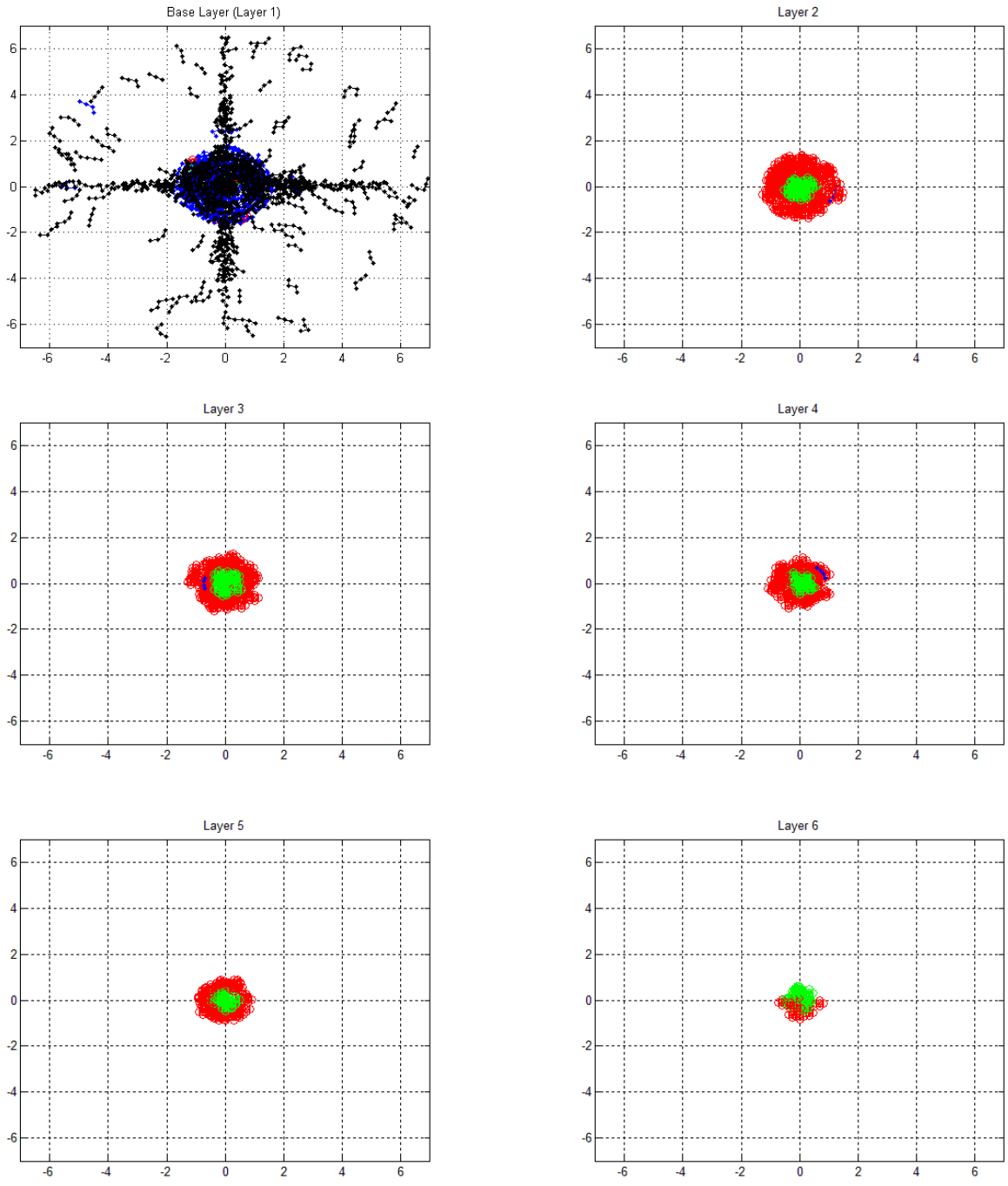

Figure 21: The internal structure of a mature fruiting body. The red spores indicate the outer spores, while the green indicate the inner spores.

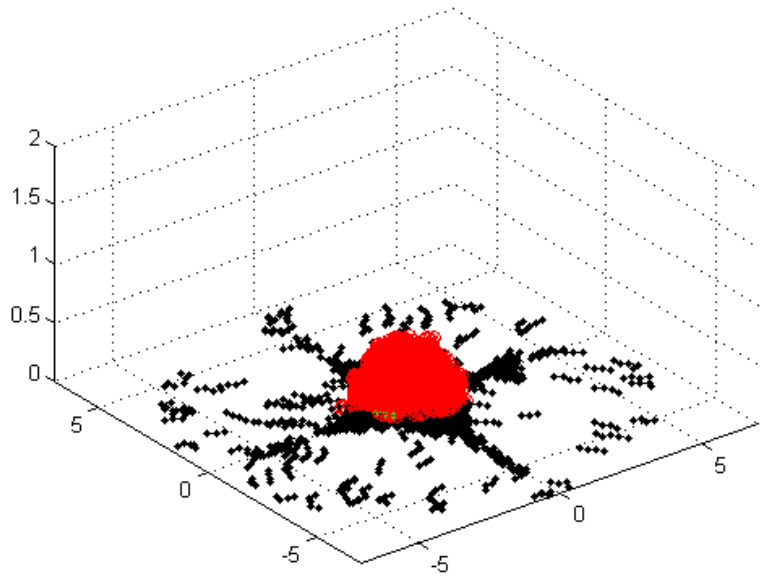

Figure 22: The three-dimensional view of a mature fruiting body consisting of myxospores. The red-colored cells are those that have differentiated into spores.

[4] A. Gallegos, B. Mazzag, A. Mogilner, *Two continuum models for the spreading of myxobacteria swarms*, Bulletin of Mathematical Biology, 837-861, 2006.

[5] T. M. Gronewold, D. Kaiser, *The act operon controls the level and time of C-signal production for Myxococcus xanthus developement*, Molecular Microbiology, 40(3), 744-756, 2001.

[6] J. Hodgkin, D. Kaiser, *Genetics of gliding motility in Myxococcus xanthus: genes controlling movement of single cells*, Mol. Gen. Genet., 171:167-176, 1979.

[7] J. Hodgkin, D. Kaiser, *Genetics of gliding motility in Myxococcus xanthus: two gene systems control movement*, Mol. Gen. Genet., 171:177-191, 1979.

[8] D. Kaiser, *Coupling cell movement to multicellular development in myxobacteria*, Nature Reviews Microbiology, 1, 45-54, 2003.

[9] D. Kaiser, C. Crosby, *Cell movement and its coordination in swarms of Myxococcus xanthus*, Cell Motility 3, 227-245, 1983.

[10] D. Kaiser, R. Welch, *Dynamics of fruiting body morphogenesis*, Journal of Bacteriology, 919-927, 2004.

[11] D. Kaiser, R. Yu, *Reversing cell polarity: evidence and hypothesis*, Cur. Opin. Microbiol., 8, 216-221, 2005.

[12] S. Kim, D. Kaiser, *Purification and properties of Myxococcus xanthus C-factor, an intercellular signaling protein*, Proc. Natl. Acad. Sci. USA, Volume 87, Number 10, 3635-3639, 1990.

[13] S. A. L. M. Kooijman, *Dynamic Energy and Mass Budgets in Biological Systems*, Cambridge University Press, Cambridge, 2000.

[14] R. M. Nisbet, E. B. Muller, K. Lika, S. A. L. M. Kooijman, *From molecules to ecosystems through dynamic energy budget models*, Journal of Animal Ecology, 69, 913-926, 2000.

[15] H. Reichenbach, *Myxobacteria II*, eds. M. Dworkin, D. Kaiser, Am. Soc. Microbiol, Washington, DC, 13-62.

[16] B. Sager, D. Kaiser, *Two cell-density domains within the Myxococcus xanthus fruiting body*, Proc. Natl. Acad. Sci. USA, 90, 3690-3694, 1993.

[17] O. Sozinova, Y. Jiang, D. Kaiser, M. Alber, *A three-dimensional model of myxobacterial aggregation by contact-mediated interactions*, Proc. Natl. Acad. Sci USA, Volume 102, Number 32, 11308-11312, 2005.

[18] O. Sozinova, Y. Jiang, D. Kaiser, M. Alber, *A three-dimensional model of myxobacterial fruiting-body formation*, Proc. Natl. Acad. Sci USA, Volume 103, Number 46, 17255-17259, 2006.

[19] H. Sun, D. R. Zusman, W. Shi, *Type IV pilus of Myxococcus xanthus is a motility apparatus controlled by the frz chemosensory system*, Current Biology, Volume 10, Number 18, 1143-1146, 2000.

[20] L. Tsimring, H. Levine, I. Aranson, E. Ben-Jacob, I. Cohen, O. Shochet, W. Reynolds, *Aggregation Patterns in Stressed Bacteria*, Phys. Rev. Lett, 75, 1859-1862, 1995.

[21] C. Wolgemuth, E. Hoiczyk, D. Kaiser, G. Oster, *How myxobacteria glide*, Curr. Biol., 12:1-20, 2002.

[22] Y. Wu, N. Chen, M. Rissler, Y. Jiang, D. Kaiser, M. Alber, *CA Models of Myxobacteria Swarming*, ACRI 2006, LNCS 4173, Springer-Verlag, Berlin, 192-203, 2006.